Analysis, Design, and Experimentation of a Dimmable Resonant-Switched-Capacitor LED Driver With Variable Inductor Control

Marco Martins, Marina S. Perdigão, *Member, IEEE*, Andre M. S. Mendes, *Member, IEEE*, Rafael A. Pinto, and J. Marcos Alonso, *Senior Member, IEEE*

***Abstract*—This paper proposes a new 48-V dc-fed dimmable LED driver based on a resonant-switched-capacitor topology (RSCT), where the analog-based dimming feature is accomplished by means of a variable inductor (VI). The proposed topology is based on the classic RSCT step-up double mode converter and it provides a simple and cost-effective solution while guaranteeing a wide dimming range. In order to implement an analog-based dimming, the control of the dc current in the LED lamp is required. This technique proposes to replace the resonant inductor by a VI, which will control the rms value of the resonant current, and, therefore, the mean value of the LED lamp current. In order to evaluate the feasibility and performance of this method, a 22-W LED lamp and driver prototypes were built. The most relevant experimental results are presented and briefly described.**

***Index Terms*—Dimming, electromagnetic devices, LED driver, LED lamps, switched-capacitor converter (SCC), variable inductor (VI).**

NOMENCLATURE

$\omega_o = 1/\sqrt{L_r C_r}$	Resonant frequency [rad/s].
ΔV_{C_r} ; ΔV_{C_o}	Resonant and output capacitors voltage ripple, respectively.
$\Delta V_{C_{r_{\text{avg}}}}$	Resonant capacitor average voltage.
$I_{\text{LEDs}_{\text{avg}}}$; $V_{\text{LEDs}_{\text{avg}}}$; R_{LEDs}	LEDs average voltage and current and static resistance for a specific operating point, respectively.
v_{L_r} ; v_{C_r} ; v_{C_o} ; i_{Cr} ; i_{C_o} ; i_{L_r}	Instantaneous voltage and current flowing through L_r; C_o and C_r.
$\Delta Q_{r_{\text{discharge}}}$; ΔQ_{C_o}	Amount of charge flowing out of C_r during the discharging process and amount of charge flowing to the load during one switching cycle.
V_d	Forward voltage during conduction [V].
V_{ds}	Mosfet drain-to-source voltage during the off state [V].
I_m	Mosfet drain-to-source current when it is switched to the off-state [A].
I_{avg}	Diodes and resistors average current [A].
R_{ds}	Mosfet in-series resistance while conducting [Ω].
R_{series}	Resistance of sense resistors and VI windings [Ω].
t_{off}	Time it takes to null the mosfet current in the off-state [s].
I_{rms}	VI main windings rms current [A].
B_p	Core flux density [mT].
V_e	Core effective volume [mm^3].
P_v	Relative core losses [kW/m^3].

Manuscript received November 24, 2015; revised February 21, 2016 and May 2, 2016; accepted May 17, 2016. Date of publication June 7, 2016; date of current version January 20, 2017. This work was supported in part by the Spanish Government under the Research Grant ENE2013-41491-R. Recommended for publication by Associate Editor C. K. Tse.

M. Martins and A. M. S. Mendes are with the Instituto de Telecomunicações, Lisboa 1049-001, Portugal, and also with the Departamento de Engenharia Electrotécnica e de Computadores, Faculdade de Ciências e Tecnologia da, Universidade de Coimbra, Coimbra 3030-290, Portugal (e-mail: marco.martins.se@gmail.com; andresm@deec.uc.pt).

M. S. Perdigão is with the Instituto de Telecomunicações, Lisboa 1049-001, and also with the ISEC, DEE, Polytechnic Institute of Coimbra, Coimbra 3045-093, Portugal (e-mail: perdigao@mail.isec.pt).

R. A. Pinto is with the Group of Intelligence in Lighting, UFSM/GEDRE, Electrical and Computational Systems Research and Develop Group, UFSM/CTISM/GSEC, Federal University of Santa Maria, Santa Maria 97105-900, Brazil (e-mail: rafael@gedre.ufsm.br).

J. Marcos Alonso is with the Electrical Engineering Department, Tecnología Electrónica, University of Oviedo, Oviedo 33003, Spain (e-mail: marcos@uniovi.es).

Color versions of one or more of the figures in this paper are available online at http://ieeexplore.ieee.org

Digital Object Identifier 10.1109/TPEL.2016.2575918

I. INTRODUCTION

RECENTLY, through the increasing use of smart electronic devices (tablets, smart phones, etc.), as well as other state-of-the-art technologies, LED drivers demand a high performance with increasing functionalities, such as universal input range, retrofit capability, dimming, and emitted color programming capabilities. These drivers also include auxiliary circuits for protection, power factor correction and harmonic standards compliance, visible light communication, remote operation or others [1]–[4]. However, an LED driver that comprises such functionalities must be an attractive and low-cost solution while accomplishing a high performance [5]. Dimming functionality, using analog or PWM techniques, is an indispensable feature for state-of-the-art LED lamps. For an intelligent and cost-effective light-management system, a reduction of the power consumption is not synonym of turning off the lights completely. Thus, developing an efficient dimming technology, while guaranteeing an adequate operation and ensuring a visual comfort has been a critical goal over the last decade for the lighting industry,

especially in LED lighting systems. The most basic dimming techniques use simple variable resistors, semiconductors, or integrated circuits in series with the LEDs to control their current. In dc–dc converter-based LED drivers, the luminous output may also be controlled by regulating the dc bus voltage, via switching frequency $f_{\rm s}$ and/or duty-cycle (d) control. In spite of being sometimes quite complex, frequency control, phase-shift, or duty-cycle modulation techniques remain the conventional employed dimming techniques due to their robustness and reliability. In [6], Pinto *et al.* propose a technique for current equalization in multiple LED strings, by including a variable inductor (VI) in the output of a forward-converter LED driver. In this case, the proposal is to control the output current applied to the LED branches independently by the same control parameter: the variable inductance. The proposed technique is consistent with analogue dimming, where the level of the LEDs current is changed according to the rms value of the resonant current. Analogue dimming is a simple technique normally selected in lighting design projects with low requirements in terms of dynamics and sensibility. In this paper, the authors propose the application of a robust low-cost multiple-output dc-fed resonant-switched-capacitor topology (RSCT), for the current control of a single or multiple branches of LED strings, also based on a VI. The proposed dimmable LED driver copes with the current trend, which is taking advantage of the rapid adoption of dc power distribution in commercial and office structures, for building automation control and, in particular, lighting control [7], [8].

II. Resonant-Switched-Capacitor Converter

Switched-capacitor converters (SCC) are dc–dc converters that use only switches and capacitors, where the latter are used as energy storage elements, by "moving" charges into and out of them, in order to provide a required output voltage value. Regarding the output–input voltage ratio, three main topologies of SCC, with various combinations of switches and capacitors, are available. They can be divided into SCC divider (step-down), inverter, or multiplier (step-up) [9]. The scope of this study is focused on a step-up-based resonant SCC.

A. Classic RSCT

The RSCT was first proposed to overcome major drawbacks of nonresonant SCC, which could then be used only in applications of low-power levels. The reason for that was their poor efficiency, hard switching with high-current spikes resulting in high EMI and low rated lifetime due to the requirement of large electrolytic capacitors [10], [11]. Resonant SCC have a peculiar and interesting feature. Particularly, for the step-up version of the converter topology, it can provide almost any fixed output/input voltage ratio. This is strongly dependent on the number of switched-capacitor cells used in its structure, as illustrated in Fig. 1(a).

In fact, this is true only when the converter is operated at or near resonance. Under such conditions, the average output voltage $V_{\rm out}$ may be given by

$$V_{\rm out} = (n+2) \cdot V_{\rm in} \tag{1}$$

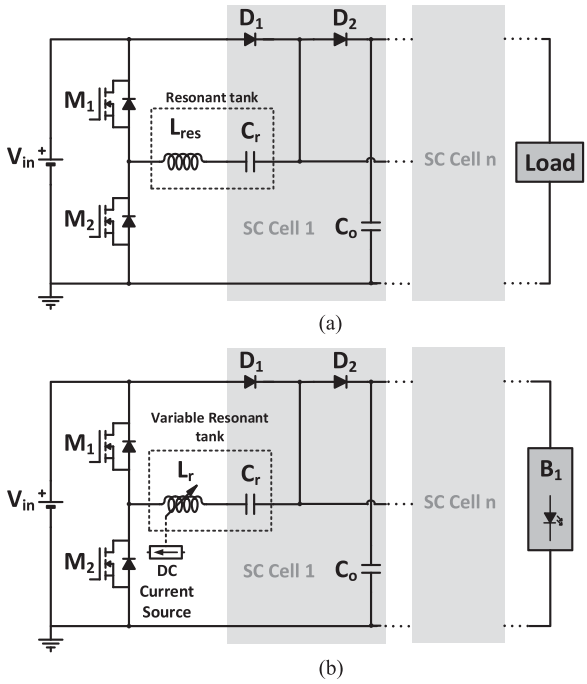

Fig. 1. RSCT: (a) Classical step-up *n*-mode; (b) VI-RSCT.

where $V_{\rm in}$ is the converter average input voltage and n is the number of additional SC cells, as illustrated in Fig. 1(a). Consequently, by cascading n SC cells, the output/input voltage ratio equals a factor of $n+2$. If $n = 1$, the step-up double mode RSCT is obtained. Under these circumstances, the output voltage equals double of input voltage.

B. RSCT: Typical Control Schemes

The RSCT operation is highly dependent on the nature of its load, which means that a proper and adequate control is mandatory to regulate its output power when connected to the LED lamp. The energy transfer is achieved by controlling the charging and discharging process of the switched capacitors. The classically employed techniques are as follows:

1) *PWM (duty-cycle control of a single switch or all switches)* [12]*:* This type of technique, however, shows that the output voltage range remains narrow and it is achieved at the expense of decreasing the converter's efficiency [13], [14]. Moreover, methods based on this technique may cause increased switching and on-state losses due to its hard switching operation and large peak current which is a source of EMI, thus leading to the decline of the conversion efficiency.
2) *Variable switching frequency* $f_{\rm s}$ [15]*:* This technique faces the same disadvantages of the previous one. In addition, it is common knowledge that a varying switching frequency raises difficulties when designing EMI filters.
3) *Phase-shift control* [14], [16]*:* This technique probably offers the best performance; however, it is quite complex requires a higher component count and most importantly, the output voltage may have a quite high undesired ripple

[14], [17]. The former issue of this technique is enough to justify the fact that it shall not be applied to converters supplying LED-based loads, since for this type of load, small voltage variations can cause high-current variations.

To cope with these former techniques issues, a new technique to regulate the operation of the RSCT is proposed using VI control.

C. Variable Inductor Resonant-Switched-Capacitor Topology

Fig. 1(b) shows the new VI-RSCT-based topology, where the VI replaces the typical resonant inductor and B_1 represents an LED branch. A branch is defined as a string of LEDs. As response to a dc control current, the global reluctance of the core is varied, and, therefore, the differential inductance of the inductor can be controlled. Thus, the circuit resonant frequency f_r will change according to the inductance value. Since its principle of operation may be found in the prior literature, it will not be further addressed in this paper [18]. Unlike former control schemes found in the prior literature, where f_r is generally kept constant while f_s is adjusted, the control technique presently proposed is based on the opposite principle: f_s (as well as d) are kept constant and f_r is varied by changing the impedance of a resonant tank, thus acting as the control variable. The constant f_s operation implies an immediate control over the switching losses. Varying f_r results on the change of the resonant current (i_r) amplitude and rms value, flowing through the VI L_r. If an LED lamp is used as load, it is possible to control the LEDs average current $I_{\mathrm{LEDs_{avg}}}$ and change the lamp luminous output. For this, it is required to obtain the relationship between L_r and the desired operation point of the LED lamp, establishing an inductance range capable of providing dimming between 30% and 100% of nominal power. The proposed technique relies on the linearity between the LEDs forward current and luminous flux, which is classified as analog dimming. When compared to PWM dimming techniques, it is a less complex solution, being generally more efficient particularly for low dimming levels. One of its key advantages is the easy control of EMI emissions [2]. Using this converter topology in conjunction with VI control is considered as an innovative technique, with high potential for low-cost dimmable LED drivers, due, not only to its originality, but also to its inherent low-power losses [19]. The following sections will present a general design procedure and implementation of a dc-fed 48-V 100-kHz LED driver based on a RSCT, to supply a 22-W LED lamp (formed by a string of 20 LEDs). The driver will be capable of performing dimming in a range of approximately 30% to 100% of nominal power, which corresponds to the safe limits of current given by the manufacturer. The operation of the VI-RSCT as well as the early stage results obtained with the experimental driver prototype will be described.

III. Dimmable LED Driver With VI Based on a RSCT

Fig. 2 shows the proposed dimmable VI-RSCT LED driver with a dual-output stage (two parallel output cells). The operation of the proposed topology is similar to the classic one: the resonant capacitors C_{r1} and C_{r2} are charged by the input voltage V_{in} and then discharged to the LED branches, B_1 and B_2, at a constant f_s and d. The output capacitors C_{o1} and C_{o2} ensure that the LED strings are still supplied when the capacitor C_{r1} and C_{r2} are being charged. The amount of power flowing to the loads is determined by both independent L_{r1} and L_{r2}. For $d = 0.5$, and if f_s is selected to be higher than f_r, switches M_1 and M_2 are softly switched on with zero voltage switching (ZVS). With lower on switching losses, high-efficiency and high-performance are accomplished. The additional benefit of the multioutput basis is that each output load can be controlled independently. This results in a high degree of freedom regarding the design of the whole driver, since it is possible to design each output to provide, equal or different output/input voltage ratios or dimming level. Hence, it is easy to provide output characteristics that meets the requirements of different branches (amount of LEDs, LEDs of different electrical characteristics, RGB-LEDs, etc.).

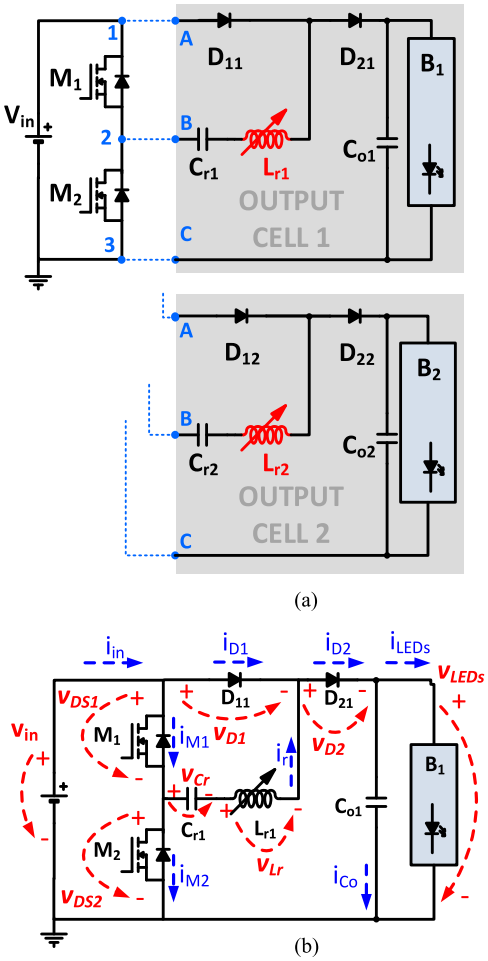

Fig. 2. Proposed dimmable VI-RSCT LED driver: (a) Dual-output stage; (b) voltages and currents convention.

A. Operating States

Fig. 3 shows the steady-state equivalent circuit of the proposed VI-RSCT and the correspondent operating states. The

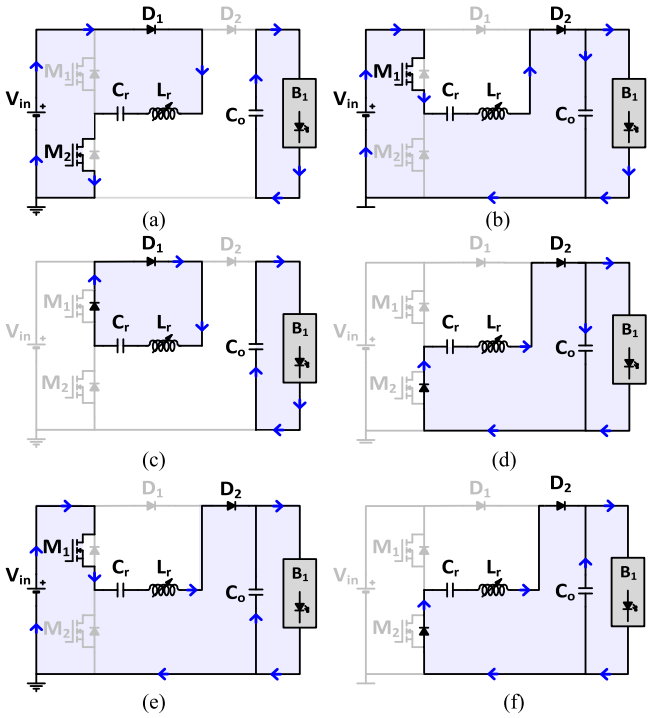

Fig. 3. Steady-state equivalent circuit and corresponding operating states of the VI-RSCT LED driver: (a) State 1 $[t_0, t_1]$; (b) State 2 $[t_1, t_2]$; (c) State 3 $[t_2, t_3]$; (d) State 4 $[t_3, t_4]$; (e) State 5 $[t_4, t_5]$; (f) State 6 $[t_5, t_0]$.

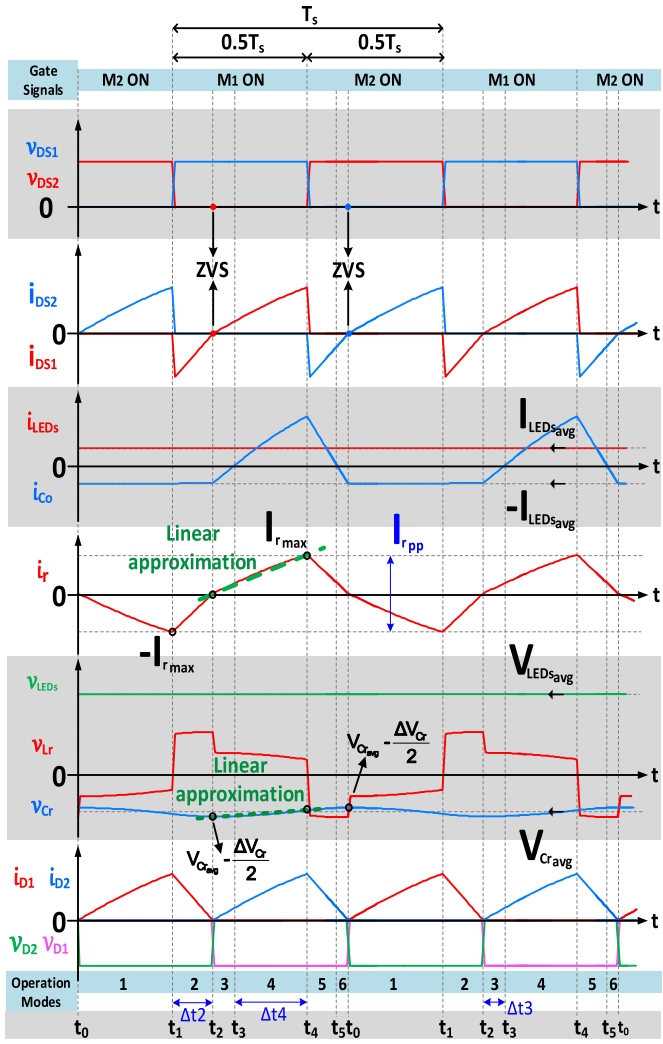

Fig. 4. Operating waveforms of the VI-RSCT.

analysis of the circuit operation assumes the following: all switching devices are ideal (no on-state voltage drop or resistance), all capacitors are ideal (no ESR), the output capacitor C_o is large enough to consider the output voltage ripple small, the input voltage V_{in} is also considered ideal; f_s is constant and the switches are turned on with ZVS.

Six states of operation are identified. During State 1 and State 2, which together last half a switching cycle, C_r is charged. During the remaining states, C_r is discharged to the load. The main theoretical waveforms of converter are shown in Fig. 4. It is important to notice that a few of these waveforms are not up to scale to each other. The states equations are presented in Table I.

Each state of operation can be described as follows:

1) *State 1:* $t \in [t_0, t_1]$: M_2 is in on-state. The resonant tank is charged by the input voltage V_{in} in a nearly resonant (sinusoidal) manner until $t = t_1$. In State 1, there is no energy transferred to the load through the resonant circuit, and, therefore, C_o is responsible for supplying energy to the load during this time. As i_r reaches zero at t_0, v_{C_r} reaches its maximum value which equals $V_{Cr_{\text{avg}}} + \Delta V_{Cr}/2$.
2) *State 2:* $t \in [t_1, t_2]$: M_1 is turned on at $t = t_1$. Due to the operation of the mode 1, and since the resonant period is larger than the switching period $T_s = 1/f_s$, there is not enough time for i_r to reach zero, thus $i_r(t_1) \neq 0$. Consequently, the antiparallel diode of M_1 conducts from $t = t_1$ until i_r drops to zero at $t = t_2$. Similarly to the State 1, C_r keeps being charged. C_o is still responsible for supplying energy to the load during this state. In State 2 equations presented in Table I, $i_r(t_1)$ is the resonant current minimum value. At $t = t_1$, the input voltage source is no longer charging the resonant tank. Together, State 1 and State 2 last half a switching cycle $(0.5\ T_s)$.
3) *State 3:* $t \in [t_2, t_3]$: M_1 is in on-state. At $t = t_2$, $i_r(t_2) = 0$ and C_r stops being charged, reaching its reverse peak voltage value $v_{C_r}(t_2)$. During this state, the energy stored in C_r is released to the load through D_2, as well as the energy stored in C_o, and, therefore, i_r will increase.
4) *State 4:* $t \in [t_3, t_4]$: State 4 is similar to State 3. i_r keeps increasing its amplitude until its maximum at $t = t_4$. At this instant, C_o is fully charged.
5) *State 5:* $t \in [t_4, t_5]$: M_1 and M_2 are both in off-state. C_r is responsible for supplying the load as well as for partially charging C_o. i_r has reached its maximum value at $t = t_4$. V_{in} is no longer connected to the remaining circuit; thus, i_r will now start to decrease due to the reduction of charge in C_r.

TABLE I
VI-RSCT STATES OF OPERATION: EQUATIONS

State 1: $t \in [t_0, t_1]$	State 2: $t \in [t_1, t_2]$	State 3: $t \in [t_2, t_3]$
$v_{C_r}(t) = -V_{in} - v_{L_r}(t)$ (2)	(4) is also valid for this state	(4) is also valid for this state
$i_{Co}(t) + i_{LEDs}(t) = 0$ (3)	$v_{C_r}(t) = -v_{L_r}(t)$ (6)	$v_{C_r}(t) = V_{in} - v_{L_r}(t) - v_{LEDs}(t)$ (9)
$i_r(t) = \frac{-v_{C_r}(t_0) - V_{in}}{\omega_o \cdot L_r} \cdot \sin \omega_o (t - t_0)$ (4)	$i_{C_o}(t) + i_{LEDs}(t) = 0$ (7)	$i_r(t) + i_{C_o}(t) = i_{LEDs}(t)$ (10)
$v_{C_r}(t) = V_{C_{avg}} + \frac{\Delta V_{C_r}}{2} \cdot \cos \omega_o (\mathrm{t} - \mathrm{t}_0)$ (5)	$i_r(t) = \frac{v_{C_r}(t_1)}{\omega_o \cdot L_r} \cdot \sin \omega_o (t - t_1)$ (8)	$i_r(t) = \frac{V_{in} - v_{C_r}(t_2) - V_{LEDs_{avg}}}{\omega_o \cdot L_r} \cdot \sin \omega_o (\mathrm{t} - \mathrm{t}_2)$ (11)

State 4: $t \in [t_3, t_4]$	State 5: $t \in [t_4, t_5]$	State 6: $t \in [t_5, t_0]$
(4), (8) and (10) are also valid for this state	(4) is also valid for this state	(4), (12) and (14) are valid for this state as well
$i_r(t) = i_{C_o}(t) + i_{LEDs_{avg}}(t)$ (12)	$v_{C_r}(t) = -v_{L_r}(t) - v_{LEDs}(t)$ (13)	$i_r(t) + i_{C_o}(t) = i_{LEDs}(t)$ (16)
	$i_r(t) = i_{C_o}(t) + i_{LEDs}(t)$ (14)	
	$i_r(t) = \frac{-v_{C_r}(t_4) - V_{LEDs_{avg}}}{\omega_o \cdot L_r} \cdot \sin \omega_o (t - t_4)$ (15)	

6) *State 6:* $t \in [t_5, t_0]$: State 6 is similar to State 5 since i_r keeps decreasing its amplitude and M_1 and M_2 are both in off-state. However, C_o is now fully charged at $t = t_5$, and, therefore, its energy will be released to the load.

B. Circuit Design Procedure

This section presents a simplified approach for the selection of the resonant tank parameters C_r , and L_r and the value of C_o . The required L_r range is determined by the maximum and minimum dimming levels. C_r , also known as the switched capacitor, is the one responsible for the energy transfer and C_o is the output filter capacitor. The voltage ripple across them affects the efficiency of power conversion as well as the stability of the output voltage. An analogue dimmed LED driver must be designed considering an output voltage and current with negligible ripple.

1) Resonant Capacitor Calculation C_r: The amount of charge flowing to C_r during the charging process (State 1 and 2) should be equal to the amount of charge flowing out of it during the discharging process (States 3, 4, 5, and 6). Assuming that C_o is ideal, the integration of i_{C_o} (equaling the amount of charge flowing into and out of it) should be equal to zero during one switching cycle. During the discharging process, the converter currents can be related by

$$i_r(t) = i_{C_o}(t) + i_{\mathrm{LEDs}}(t). \tag{17}$$

The amount of charge flowing out of C_r during the discharging process, $\Delta Q_{r_{\mathrm{discharge}}}$ (given by (18)), from $t_2 = T_s\ /2$ to $t_0 = T_s$ should be equal to the amount of charging flowing to the load during one switching cycle, ΔQ_{C_o} (given by (19)), as shown in (20)

$$\Delta Q_{r_{\mathrm{discharge}}} = \Delta V_{Cr} \cdot C_r = \int_{T_s/2}^{T_s} i_r(t)dt = \frac{T_s}{4} \cdot I_{r\_\max} \tag{18}$$

$$\Delta Q_{C_o} = \int_0^{T_s} i_{\mathrm{LEDs}}(t)dt = I_{\mathrm{LEDs_{avg}}} \cdot T_s. \tag{19}$$

The required capacitance of C_r can be obtained using (20). Equaling (18) to (19) results into (20) and (21)

$$\Delta V_{C_r} \cdot C_r = I_{\mathrm{LEDS_{avg}}} \cdot T_s \tag{20}$$

$$I_{r\_\max} = 4 \cdot I_{\mathrm{LEDs_{avg}}}. \tag{21}$$

2) Output Capacitor Calculation C_o: The amount of charge flowing to the load during one switching cycle, ΔQ_{C_o} can be defined using (22), from which C_o can be also determined

$$\Delta Q_{C_o} = \Delta V_{C_o} \cdot C_o = \int_0^{T_s/2} i_{C_o}(t)dt. \tag{22}$$

During the charging process, from $t_0 = 0$ to $t_2 = T_s\ /2$, the current flowing through the output capacitor is the same to that flowing through the LEDs load as shown in

$$i_{C_o}(t) = i_{\mathrm{LEDs}}(t). \tag{23}$$

Whereas during the discharging process, the current through the output capacitor can be given by (24), which is obtained from reorganizing the members of (17)

$$i_{C_o}(t) = i_r(t) - i_{\mathrm{LEDs}}(t). \tag{24}$$

Assuming i_{LEDs} as constant, i.e., with a neglected ripple, and substituting (24) into (22) during the discharging period of time, (25) is obtained, from which the required capacitance of the output capacitor may be calculated

$$C_o = \frac{3 \cdot T_s \cdot I_{\mathrm{LEDs_{avg}}}}{4 \cdot \Delta V_{C_o}}. \tag{25}$$

3) Variable Inductance Range Calculation: The design of the VI range is based on the determination of two static values of inductance, namely the minimum and maximum required values. A linear approximation method to determine such values is presented. Since it is a quite empirical method, a few assumptions are used: the output capacitor is large enough so that its voltage ripple can be neglected. Hence, the output voltage v_{LEDs} can be assumed as a constant voltage source $V_{\mathrm{LEDs_{avg}}}$; f_s is high enough to satisfy the condition $f_s \gg f_r$ so that the

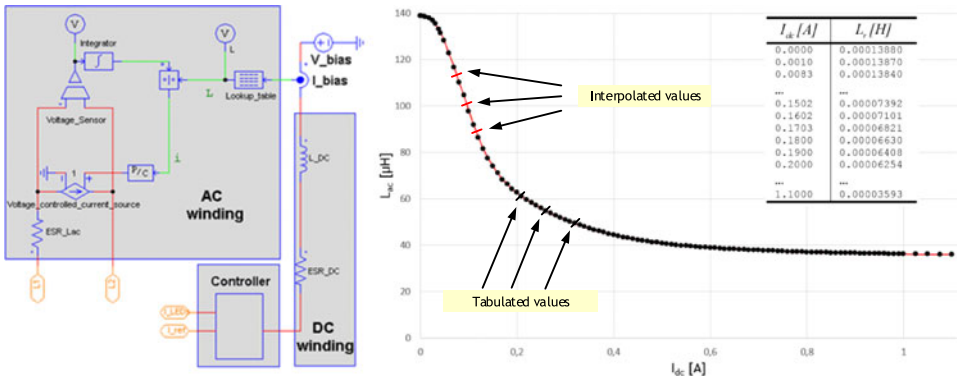

(a) (b)

Fig. 5. VI model: (a) Schematic of the VI model in PSIM; (b) lookup table simplified file and graphic representation of the linear interpolation of the VI characteristic.

changes on the resonant current (i_r) can be approximated as linear in time.

First, considering that the resonant current reaches its maximum value at t_4, and that during States 3 and 4, the resonant capacitor average voltage is $V_{Cr_{3,4}}$, eq. (12), may be linearly approximated as shown in (26), where $I_{r_{\max}}$ is given by (21), $V_{Cr_{3,4}}$ is estimated and may be given by (27) and $(t_4 - t_2)$ given by (28)

$$i_r(t_4) = I_{r_{\max}} = \frac{V_{\text{in}} - V_{Cr_{3,4}} - V_{\text{LEDs}_{\text{avg}}}}{L_r} \cdot (t_4 - t_2) \quad (26)$$

$$V_{Cr_{34}} = V_{Cr_{\text{avg}}} - \frac{\Delta V_{Cr}}{4} \quad (27)$$

$$t_4 - t_2 = \Delta t_3 + \Delta t_4. \quad (28)$$

In (27), ΔV_{Cr} can be obtained by (20), while $V_{Cr_{\text{avg}}}$ can be easily determined by integrating v_{Cr} during one full switching cycle as shown in

$$V_{Cr_{\text{avg}}} = \frac{1}{T_s} \cdot \int_0^{T_s} v_{Cr}(t)dt. \quad (29)$$

Substituting (3), (7), (10), and (14) into (29), results in the relation which gives the value of $V_{Cr_{\text{avg}}}$, as shown in

$$V_{Cr_{\text{avg}}} = -\frac{V_{\text{LEDs}_{\text{avg}}}}{2}. \quad (30)$$

On the one hand, in (26), the $(t_4 - t_2)$ period of time corresponds to the elapsed time during States 3 and 4, which can be given by (28). Δt_3 and Δt_4 are the period of time that the States 3 and 4 last, respectively. On the other hand, States 2, 3, and 4 together last half a switching cycle as shown in (31), where Δt_4 is the elapsing time of State 2

$$\Delta t_2 + \Delta t_3 + \Delta t_4 = \frac{T_s}{2} \Leftrightarrow \Delta t_3 + \Delta t_4 = \frac{T_s}{2} - \Delta t_2. \quad (31)$$

In (31), Δt_2 is determined by recalling (7) for State 2 $(t_1 - t_2)$ and knowing that at t_1, the resonant current reaches its negative peak value $(i_r(t_1))$, which in turn equals to $-I_{r_{\max}}$. At $t = t_2$, when i_r reaches zero, v_{Cr} also reaches its negative peak value $v_{Cr}(t_2)$ which is given by (32), and which in turn is obtained for $t = t_2$ by substituting (30) into (6)

$$v_{Cr}(t_2) = V_{Cr_{\text{avg}}} - \frac{\Delta V_{Cr}}{2} = -\frac{V_{\text{LEDs}_{\text{avg}}} + \Delta V_{Cr}}{2}. \quad (32)$$

Recalling (7) and using a linear approximation for i_r as shown in Fig. 4 ($v_{Lr} = L_r\, di/dt$) and that $i_r\,(t_1) = -I_{r_{\max}}$, (32) may be rewritten as shown in

$$-v_{Cr}(t_2) = \left(L_r \cdot \frac{-i_r(t_1)}{\Delta t_2}\right). \quad (33)$$

Reorganizing (33) in order to isolate Δt_2, and substituting (32) into it, (34) is obtained

$$\Delta t_2 = \frac{8 \cdot L_r \cdot I_{\text{LEDs}_{\text{avg}}}}{V_{\text{LEDs}_{\text{avg}}} + \Delta V_{Cr}}. \quad (34)$$

Finally, combining (21), (27), (31), and (34) into (26), a relation that can give the value of the inductance, necessary for a determined dimming level, is finally obtained. This relation is presented in (35), where V_a and V_b are given by (36) and (37), respectively

$$L_r = \frac{(V_a) \cdot (V_b)}{(8 \cdot f_s \cdot I_{\text{LEDs}_{\text{avg}}}) \cdot [2 \cdot (V_a) + (V_b)]} \quad (35)$$

$$V_a = V_{\text{in}} - \frac{V_{\text{LEDs}_{\text{avg}}}}{2} + \frac{I_{\text{LEDs}_{\text{avg}}}}{4 \cdot f_s \cdot C_r} \quad (36)$$

$$V_b = V_{\text{LEDs}_{\text{avg}}} + \frac{I_{\text{LEDs}_{\text{avg}}}}{f_s \cdot C_r}. \quad (37)$$

IV. Simulation

A. VI Modeling

Simulation is particularly useful when it is necessary to deal with a nonlinear behavior that cannot be easily handled analytically.

To some extent, the VI might show a nonlinear behavior, which can affect some parameters of the converter, such as the inrush current, magnitude of the load current ripple, small-signal transfer functions along with others. Nevertheless, the fact that the behavior is nonlinear is not a problem from the experimental point of view in terms of flux output, because

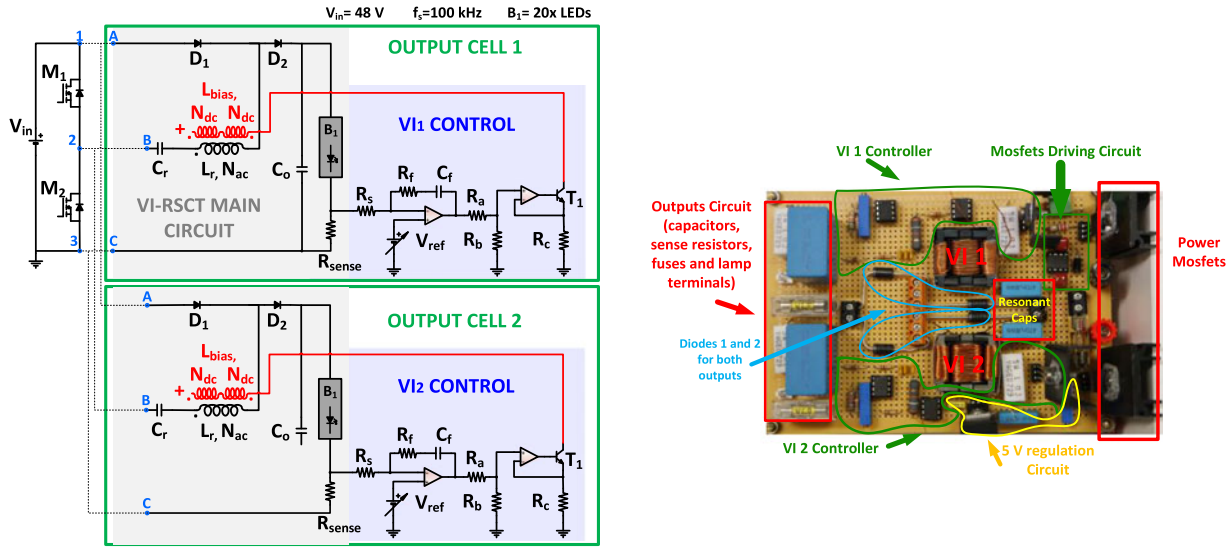

(a) (b)

Fig. 6. Schematic diagram of the laboratory prototype: (a) VI RSCT with dual output; (b) prototype.

TABLE II
DESCRIPTION OF THE MAIN PARAMETERS AND COMPONENTS USED IN THE PROTOTYPE

Description	Specification
Main Parameters	$V_{\rm in} = 48$ V, $f_s = 100$ kHz, $d = 0.5$
Switches	MOSFET IRF520, 9.2 A, 100 V, 0.27 Ω
Diodes	BYC5D 500
Resonant Capacitor	$C_r = 0.47\ \mu$F, 100 V
Variable Inductor	$L_r = 40\ \mu$H $-150\ \mu$H, $N_{\rm ac} = 35$, $N_{\rm dc} = 71$, EFD 25/13/9; air gap $= 0.6$ mm
Output Capacitor	$C_o = 10\ \mu$F, 250 V
LED Branch (B_1)	$B_1 = 20 \times$ Golden Dragon Plus, 5000 K,
LED Branch (B_1)	3.2 V, 350 mA
Opamps	LM358
Resistors—0.5 W	$R_{\rm sense} = 1\ \Omega$, $R_c = 1\ \Omega$
Resistors—0.25 W	R_s, $R_b = 10$ kΩ, $R_f = 20$ kΩ, $R_a = 39$ kΩ
Feedback Capacitor	$C_f = 3$ nF
Transistor	T_1 = BD139, n-p-n
Reference Voltage	$V_{\rm ref}$ = 100–350 mV

the change in the inductance values is done in a continuous manner. For simulation purpose, a simple and dynamic model of the VI was developed in PSIM software. The VI schematic is presented in Fig. 5 as well as the graphic representation of the linear interpolation of the VI characteristic

1) Lookup Table Model: The model is based on the small-signal characteristic measured with an LCR meter from a real VI constructed in laboratory, which will be further presented. For double E VI topologies, the value of the inductance decreases with the increase of the dc control current. The prototype characteristic is presented in the following section. The resulting model does not contain core losses, temperature effect, frequency dependence of the permeability, or the hysteresis effect. Nevertheless, it models the small-signal behavior of the prototype as response to the dc control current and it is capable of providing sufficiently accurate simulating results to verify this type of control on the LED driver.

Essentially, the VI model is based on a Lookup Table (using a .txt file). This table contains the main winding inductance value as a function of the dc control current, $L_r = f(I_{\rm dc})$. It consists of two data arrays stored in a file, one for the input $I_{\rm dc}$ and the other for the output L_r. The input array $I_{\rm dc}$ is, as required, monotonically increasing. Between two points, a simple linear interpolation is used to obtain the output. The data stored consists of two rows; the first one corresponds to the input and the second to the output. In this case, the *lookup table* approximates a 1-D function using the specified lookup method (*interpolation-extrapolation* method).

This method performs a linear interpolation and extrapolation of the inputs, these inputs being the dc control current values. This value is obtained using a current sensor in the dc (bias) winding. Using the specified method, the lookup table block automatically outputs the inductance value.

2) DC and Main Winding Models: The dc winding is simulated by means of a 1.3-Ω equivalent resistance (ESR_dc) in series with a 1.5-mH inductor. The winding is supplied with a 5-V voltage source. The main winding is simulated by means of a voltage-controlled current source in series with an equivalent series resistance (ESR_Lac). In this winding, the resonant current is defined to flow from the negative terminal to the positive terminal of the VCCS. In order to obtain and control the inductor (resonant) current, its voltage is measured first with a voltage sensor and then integrated. The result is then divided by the inductance value given by the lookup table and the inductor current is thus obtained. This process may be mathematically described as follows:

$$i_{L_r}(t) = \frac{1}{L_r(I_{\rm dc})} \int v_{L_r} \cdot dt. \tag{38}$$

TABLE III
LOSSES ANALYSIS

Component	Model	$V_{\rm d}$ [V]	$V_{\rm ds}$ [V]	$I_{\rm m}$ [A]	$I_{\rm avg}$ [A]	$R_{\rm ds}$ [Ω] at 60 °C	$R_{\rm series}$ [Ω]	$t_{\rm off}$ [s]	Losses [W]
D_1	BYC5D 500	1.1			0.35				0.39
D_2	BYC5D 500	1.1			0.35				0.39
M_1 conduction	IRF520	0.6				0.338			0.11
M_1 Turn-off	IRF520		48	1.22				$2*10^{-8}$	0.02
M_2 conduction	IRF520	0.6				0.338			0.11
M_2 Turn-off	IRF520		48	1.29				$2*10^{-8}$	0.02
$R_{\rm sense}$					0.35		1		0.12
VI element	Type	$R_{\rm series}$ [Ω]	$I_{\rm rms}$ [A]	$B_{\rm p}$ [mT]	$V_{\rm e}$ [mm^3]	$P_{\rm v}$ [kW/m^3]			Losses [W]
$L_{\rm r}$-copper	35 turns	0.3	0.798						0.19
$L_{\rm r}$-core	EFD25 N87			200	3300	300			0.99
								Total Losses [W]:	2.33
								Input Power [W]:	25.03
								Output Power [W]:	22.7
								Estimated efficiency [%]:	90.68

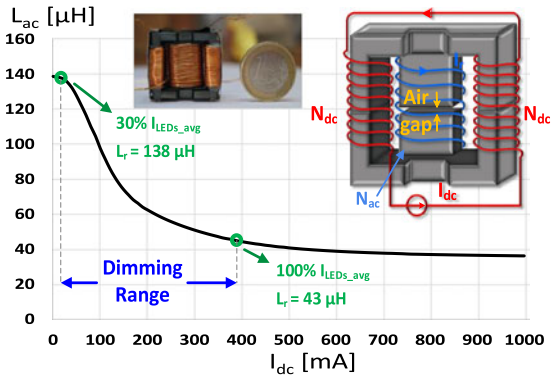

Fig. 7. VI Small-signal characteristic: ac winding's inductance ($L_{\rm ac}$) versus dc winding schematic diagram of the laboratory prototype: VI-RSCT.

V. PROTOTYPE AND EXPERIMENTAL RESULTS

In order to validate the proposed topology, simulations in PSIM were carried out and a 48-V dc-fed dimmable LED driver prototype, with a single output stage, was built and tested. The schematic, considering a dual-output, the prototype, and the remaining parameters can be observed in Fig. 6 and Table II, respectively.

Table III presents an estimation of the losses expected for the driver and the VI. This estimation is based on the information given in the datasheet of the selected components, properties of the magnetic material of the core (relative core losses versus frequency, effective core parameters), and in the simulation.

For the present case, the maximum and minimum dimming levels of the RSCT, which correspond to $i_{\rm LEDs}$ from 105 to 350 mA (from 30% to 100%), respectively, require a variable inductance L_r of 43 and 138 µH, respectively**.** These values are obtained following the design procedure presented in Section III-B. The design procedure was adopted for both outputs. The values of C_r and C_o were also obtained according to the presented procedure. In particular, the value for C_o was obtained from (25) as follows: the maximum output voltage variation (ripple) was selected to be 0.5% of the expected average output voltage

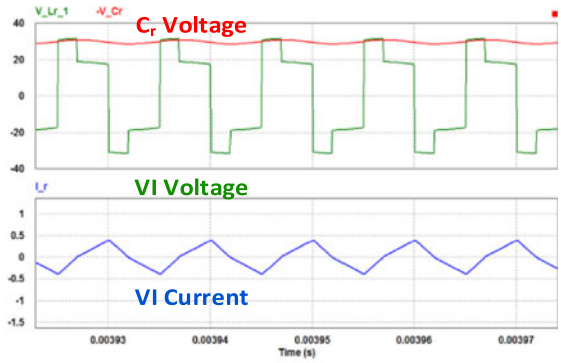

(a)

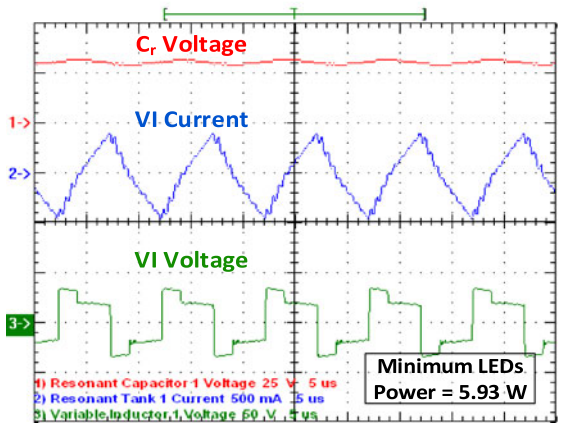

(b)

Fig. 8. v_{Cr} (inverted), i_r and v_{Lr} for minimum diming level, red, blue, and green curves, respectively: (a) simulated, (b) experimental results, 25 V/div, 0.5 A/div, and 50 V/div, respectively, 5 µs/div.

$\Delta V_{C_o} = 0.5\% \times V_{C_o}$ being $V_{C_0} = 64\ {\rm V} = N_{\rm LEDS} \times 3.2\ {\rm V}$, where $N_{\rm LEDS}$ corresponds to the number of LEDs in a string. The LED lamp was built using a string of 20 LEDs of 350 mA and 3.2 V. The remaining parameters where $f_s = 100\ {\rm kHz}$ and $I_{\rm LEDs_{av}} = 0.35$ which is the expected maximum average current flowing through the LEDs. This gives a value of 8.2 μf,

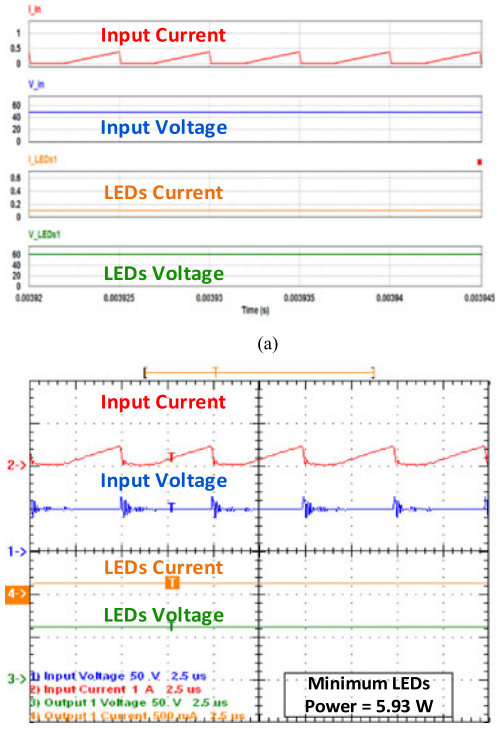

Fig. 9. Input current and voltage, i_{LEDs} and v_{LEDs} for minimum dimming level conditions, red, blue, orange, and green curves, respectively: (a) Simulated, (b) experimental results, 1 A/div, 50 V/div, 0.5 A/div, 50 V/div respectively, 2.5 µs/div.

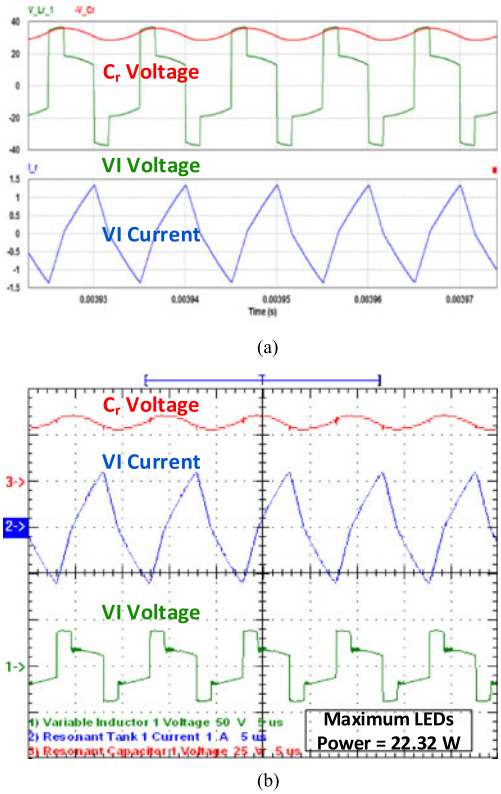

Fig. 10. v_{Cr} (inverted), i_r, and v_{Lr} for maximum diming level, red, blue, and green curves, respectively: (a) simulated, (b) experimental results, 25 V/div, 0.5 A/div, and 50 V/div, respectively, 5 µs/div.

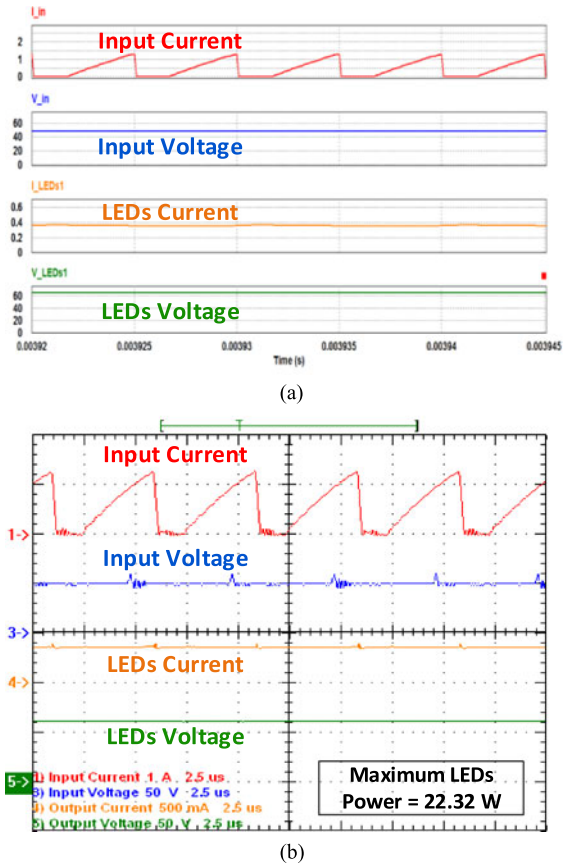

Fig. 11. Input current and voltage, i_{LEDs} and v_{LEDs} for maximum dimming level conditions, red, blue, orange, and green curves, respectively: (a) simulated, (b) experimental results, 1 A/div, 50 V/div, 0.5 A/div, 50 V/div, respectively, 2.5 µs/div.

and, therefore, the nearest commercial available value is 10 μf as selected.

The VI was designed using the methodology provided in [20] and it was built using a EFD 25 ferrite core set to form an assembly as the one sketched in Fig. 7. The relationship between the control current (I_{dc}) flowing through the control winding (L_{bias}) and the inductance value of the main winding (L_r) is shown in Fig. 7 as well. The sketched curve was obtained for one of the VIs under small-signal conditions using a *LCR* meter. The control winding was fed by a dc current source and the inductance was measured at the terminals of the main winding. This inductance is a function of the permeability of the core and this permeability depends on the level of core saturation imposed by the dc current. In the driver itself, through the implementation of a simple analogue control it is possible to increase or decrease the level of control current so that the value of the inductance will change accordingly. This adjustment can be made for each VI in both outputs, without extra complications as long as the VIs are designed with an appropriated (sufficient) inductance range to accommodate small differences in the behavior of each LED string. In [18], the fundamentals basic operating principle of such devices are described and an overview of existing topologies, patents, and applications is

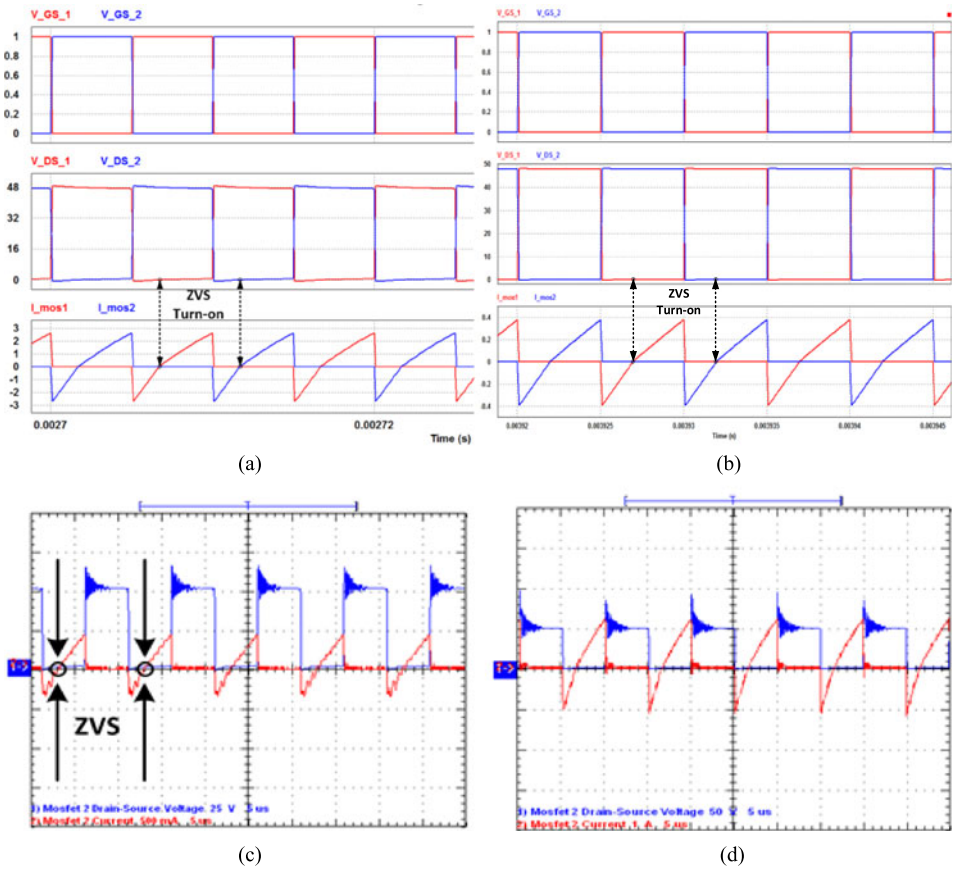

Fig. 12. ZVS during turn-on transitions. Simulated results, upper chart—gate signals, center chart—drain to source voltage, lower chart—drain to source current: (a) maximum power, (b) minimum power. Experimental waveforms, 0.5 A/div, 25 V/div, and 1 A/div, 50 V/div, respectively, 5 μs/div, drain to source voltage in blue and drain to source current in red: (c) maximum power, (d) minimum power.

presented. For further reference, in [22], a simple design procedure and a finite-element analysis of a VI model based on this exact prototype is presented.

The output current control of the converter for each cell was provided through the control of the bias winding of the VI using the hardware and analogue controller proposed in [6] including a sense resistor, an error amplifier/comparator, and a voltage follower as shown in Fig. 6(a). The output current reference, in the range of 100 to 350 mA was obtained through a simple variable voltage divider.

Figs. 8 to 11 present simulation and laboratory waveform results obtained from the experimental prototype. Both outputs presented similar results. Figs. 8 and 10 show the waveforms corresponding to v_{Cr} and v_{Lr} as well as i_r. From these figures, it is clear the variation in the peak-to-peak value of the resonant current for the two extremes of the dimming range, namely minimum and maximum levels. This confirms that it is possible to regulate the resonant current using the VI between a maximum and minimum rms value. This regulation results in different dc levels for the LEDs current, validating the main objective of this study (luminous flux regulation). In Figs. 9 and 11 are shown both input and load (LEDs) voltages and currents. The lamp current, i_{LEDs} presents a very good dc shape, practically without ripple. This constitutes a major benefit for LEDs because it eliminates any possibility of fluctuation in the luminous flux level, which could be annoying from the user point of view. This technique together with a proper heat-sink design of the luminaire and operating temperature, optimal operation conditions can be attained. Analogously to the converter presented in [21], operating the converter above the resonance leads to ZVS. ZVS is essential to ensure minimal losses during the switches turn-on process and can be observed in Fig. 12 for both simulated and experimental waveforms for maximum and minimum power levels. In general, a good agreement is shown between both simulation and experimental results obtained from the prototype. This implies that the VI model is appropriate to validate the control technique. Compared to other techniques that are more complicated [23], this is a clear advantage since the operating point of each string can be adjusted in a dedicated manner depending on the characteristics of the LED string.

Fig. 13(a) shows the prototype's dimming characteristic, consisting on the LEDs average power (lamp power) as response to the VI control current. It is noticeable a linear and smooth dimming curve, revealing this VI resonant-based topology as promising. The current, and not yet optimized, electrical conversion efficiency of the prototype assembled ranges from $\approx$88% to 94% for an output mean power range of $\approx$6 to 22 W corresponding to the selected dimming range. ZVS feature is

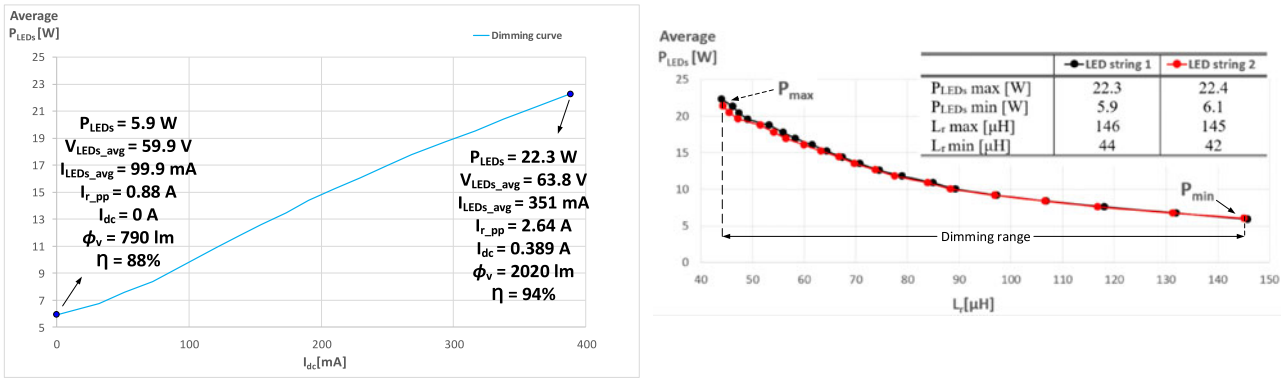

Fig. 13. Dimming curve: (a) LED string power versus VI control current; (b) dual-output LED string power versus L_r.

verified across the entire dimming range. Also, using diodes D_1 and D_2 instead of controllable switches ensures a lower component count and complexity and a higher power density. Fig. 13(b) shows the prototype's output power versus L_r characteristic for both cells. It is visible the inverse proportionality between these two parameters resulting in the linear characteristic $P(I_{dc})$.

VI. Conclusion

Based on the respective merits of the RSCT and the VI, a new cost-effective dimmable LED driver is proposed. The main circuit operation was analyzed. Simulation and practical experiments were conducted in order to validate the theoretical analysis, the effectiveness, and feasibility of the converter. The simulation results showed a very good agreement with experimental results. The VI integration gives, not only the possibility to perform dimming over wide ranges as it has been shown, but may further be used for current equalization in multiarray-based LED lamps.

In addition, by using the VI the usual coupling between input and output voltage of SCC is eliminated. In most of these converters (resonant or nonresonant), with fixed and periodic gate signals, the conversion ratio V_{out}/V_{in} is constant, which is often undesirable. The results indicate that the performance reached reasonably good levels over the whole set dimming range with a very good efficiency and with a very low-output voltage and current ripple, ensured without the need of output filtering techniques.

References

[1] C. Yao, C. Changyuan, and Y. Penglin, "A novel primary-side controlled universal-input AC-DC LED driver based on a source-driving control scheme," *IEEE Trans. Power Electron.*, vol. 30, no. 8, pp. 4327–4335, Aug. 2015.

[2] D. G. Lamar, M. Arias, M. M. Hernando, and J. Sebastian, "Using the loss-free resistor concept to design a simple AC-DC HB-LED driver for retrofit lamp applications," *IEEE Trans. Ind. Appl.*, vol. 51, no. 3, pp. 2300–2311, May/Jun. 2015.

[3] C. Yu, Z. Zhihao, and K. Yong, "Design and implementation of a transformerless single-stage single-switch double-buck converter with low DC-link voltage, high step-down, and constant input power factor features," *IEEE Trans. Power Electron.*, vol. 29, no. 12, pp. 6660–6671, Dec. 2014.

[4] K. Modepalli and L. Parsa, "Dual-purpose offline LED driver for illumination and visible light communication," *IEEE Trans. Ind. Appl.*, vol. 51, no. 1, pp. 406–419, Jan./Feb. 2015.

[5] C. Yoo-Chae, L. Kyung-Min, C. Hyung-Jin, S. Chang-Hyeon, and K. Bongkoo, "Low-cost drive circuit for AC-direct LED lamps," *IEEE Trans. Power Electron.*, vol. 30, no. 10, pp. 5776–5782, Oct. 2015.

[6] R. A. Pinto, J. M. Alonso, M. S. Perdigao, M. F. da Silva, and R. N. do Prado, "A new technique to equalize branch currents in multiarray LED lamps based on variable inductors," *IEEE Trans. Ind. Appl.*, vol. 52, no. 1, pp. 521–530, Jan./Feb. 2016.

[7] G.-S. Seo, B.-H. Cho, and K.-C. Lee, "DC level dimmable LED driver using DC distribution," in *Proc. IEEE Energy Convers. Congr. Expo.*, 2013, pp. 4650–4654.

[8] G. Seo, H. Kim, K. Lee, S. Choi, and B. Cho, "DC level dimmable LED driver with primary side on-time control for DC distribution," *IEEE J. Emerg. Sel. Topics Power Electron.*, vol. 3, no. 3, pp. 624–632, Sep. 2015.

[9] K. W. E. Cheng, "New generation of switched capacitor converters," in *Proc. IEEE 29th Annu. Power Electron. Spec. Conf. Rec.*, 1998, vol. 2, pp. 1529–1535.

[10] K. K. Law, K. W. E. Cheng, and Y. P. B. Yeung, "Design and analysis of switched-capacitor-based step-up resonant converters," *IEEE Trans. Circuits Syst. I, Reg. Papers*, vol. 52, no. 5, pp. 943–948, May 2005.

[11] Y. P. B. Yeung, K. W. E. Cheng, S. L. Ho, K. K. Law, and D. Sutanto, "Unified analysis of switched-capacitor resonant converters," *IEEE Trans. Ind. Electron.*, vol. 51, no. 4, pp. 864–873, Aug. 2004.

[12] Q. Dongyuan, Z. Bo, and Z. Chunfang, "Duty ratio control of resonant switched capacitor DC-DC converter," in *Proc. 8th Int. Conf. Electr. Mach. Syst.*, 2005, vol. 2, pp. 1138—1141.

[13] M. S. Makowski, "Voltage regulation in switched-capacitor converters—A problem revised," presented at the 5th Eur. Space Power Conf., Tarragona, Spain, 1998.

[14] S. Kiratipongvoot, T. Siew-Chong, and A. Ioinovici, "Phase-shift interleaving control of variable-phase switched-capacitor converters," *IEEE Trans. Ind. Electron.*, vol. 60, no. 12, pp. 5575–5584, Dec. 2013.

[15] M. Shoyama and T. Ninomiya, "Output voltage control of resonant boost switched capacitor converter," in *Proc. Power Convers. Conf.*, Nagoya, Japan, 2007, pp. 899–903.

[16] K. Sano and H. Fujita, "Improving dynamic performance and efficiency of a resonant switched-capacitor converter based on phase-shift control," in *Proc. IEEE Energy Convers. Congr. Expo.*, 2009, pp. 3509–3515.

[17] Taufik and J. J. Mullins, "Parallel operation of hybrid loaded resonant converter using phase-shift control," in *Proc. IEEE Int. Symp. Ind. Electron.*, 2006, pp. 988–992.

[18] M. S. Perdigao, M. F. Menke, A. R. Seidel, R. A. Pinto, and J. M. Alonso, "A review on variable inductors and variable transformers: Applications to lighting drivers," *IEEE Trans. Ind. Appl.*, vol. 52, no. 1, pp. 531–547, Jan./Feb. 2016.

[19] M. Martins, M. S. Perdigao, A. S. Mendes, R. A. Pinto, and J. M. Alonso, "Dimmable LED driver with variable inductor based on a resonant switched-capacitor topology," in *Proc. IEEE Energy Convers. Congr. Expo.*, Sep. 20—24, 2015, pp. 5329–5336.

[20] M. S. Perdigao, J. M. Alonso, M. A. Dalla Costa, and E. S. Saraiva, "Comparative analysis and experiments of resonant tanks for magnetically controlled electronic ballasts," *IEEE Trans. Ind. Electron.*, vol. 55, no. 9, pp. 3201–3211, Sep. 2008.
[21] J. M. Alonso, M. S. Perdigao, D. G. Vaquero, A. J. Calleja, and E. S. Saraiva, "Analysis, design, and experimentation on constant-frequency DC-DC resonant converters with magnetic control," *IEEE Trans. Power Electron.*, vol. 27, no. 3, pp. 1369–1382, Mar. 2012.
[22] M. S. Perdigao, S. F. Ferreira, M. Martins, A. S. Mendes, and J. M. Alonso, "Finite element analysis of a variable inductor for an RSCC based LED lamp driver," in *Proc. Ind. Appl. Soc. Annu. Meet.*, Oct. 18–22, 2015, pp.1–8.
[23] R. Zhang and H. S.-H. Chung, "Use of daisy-chained transformers for current-balancing multiple LED strings," *IEEE Trans. Power Electron.*, vol. 29, no. 3, pp. 1418–1433, Mar. 2014.

Marco Martins was born in Coimbra, Portugal, in 1990. He received the B.S. and M.S. degrees in electrical and computer engineering from the University of Coimbra, Coimbra, in 2015. During his Master's degree, he collaborated with the Associate Laboratory Instituto de Telecomunicações, Coimbra, doing research in the LED lighting domain.

Since 2015, he has been an Automation Engineer at Ekoland Sp. z o.o., Maspex Wadowice Group, Tychy, Poland. He is the Author and Coauthor of two highly referenced IEEE conference articles. His research interests include variable inductors and transformers, wireless energy transfer, switched-capacitor converters, aeronautical systems, dc-distribution systems, LED lighting, visible-light communication, PV, and wind energy control.

Mr. Martins is qualified by the Polish Association of Electrical Engineers (SEP) with a SEP license up to 1 kV.

Marina S. Perdigão (S'06–M'12) was born in Coimbra, Portugal, in 1978. She received the M.Sc. and Ph.D. degrees in electrical engineering from the University of Coimbra, Coimbra, in 2004 and 2012, respectively.

From 2006 to 2012, she conducted her Ph.D. work with the University of Coimbra in co-operation with the University of Oviedo, Oviedo, Spain. She has been with the Polytechnic Institute of Coimbra–Coimbra Institute of Engineering, Coimbra, since 2002, first as a Teaching Assistant and then as an Assistant Professor since 2012. She has been a Researcher at the Instituto de Telecomunicações, Coimbra, since 2001. She is the Coauthor of more than 50 journal and conference publications, including 13 publications in highly referenced journals. Her research interests include high-frequency electronic ballasts, discharge lamp modelling, high-frequency switching converters, resonant converters, dc–dc converters, power electronics for renewable energies, IPT, and computer simulation applications.

Dr. Perdigão has received the best paper award of the 2009 IEEE International Symposium on Industrial Electronics and was awarded by the Industrial Lighting and Display Committee of the IEEE Industry Applications Society a First Prize Paper for the technical competence displayed. She collaborates as a transactions paper reviewer as a IEEE Member.

Andre M. S. Mendes (S'95–M'05) was born in Portugal. He received the Electrical Engineering Diploma, and the M.Sc. and Dr. Eng. degrees from the University of Coimbra, Coimbra, Portugal, in 1993, 1998, and 2005, respectively.

Since 1991, he has been with the Department of Electrical and Computer Engineering, University of Coimbra, where he is currently an Assistant Professor and the Director of the Power Electronics Laboratory. He is also the Coordinator at the Power Systems Research Group, Instituto de Telecomunicações, Coimbra. His teaching interests include electrical machines and power electronics, and his research interests include electric power quality, and fault diagnosis and fault tolerance of electric drives and power electronic converters.

Dr. Mendes is a Member of the Portuguese Engineers Association.

Rafael A. Pinto was born in Santa Maria, Brazil, in 1984. He received the B.S., M.Sc., and Ph.D. degrees in electrical engineering from the Federal University of Santa Maria (UFSM), Santa Maria, in 2007, 2008, and 2012, respectively.

In 2014, he was with the University of Oviedo, Spain, as a Postdoctoral Research Scholar. Since 2009, he has been with UFSM as a Professor at the Industrial Technical College of Santa Maria. He has been a Researcher of GEDRE—Electronic Ballast Research Group, and GSEC—Electrical and Computational Systems Research and Develop Group since 2002 and 2010, respectively. His main research interests include electronics ballast and drivers for light-emitting diode.

J. Marcos Alonso (S'94–M'98–SM'03) received the M.Sc. and Ph.D. degrees in electrical engineering from the University of Oviedo, Oviedo, Spain, in 1990 and 1994, respectively.

Since 2007, he has been a Full Professor at the Electrical Engineering Department, University of Oviedo. He is the holder of seven Spanish patents. He is a Coauthor of more than 350 journal and conference publications, including 85 publications in highly referenced journals. His research interests include electronic lighting, dc–dc converters, resonant inverters, and single-phase high-frequency switching converters in general.

Prof. Alonso received the Early Career Award of the IEEE IES in 2006. He was honored with the University of Oviedo Electrical Engineering Doctorate Award for 1996. He also holds five IEEE paper awards. He serves as an Associate Editor of the IEEE TRANSACTIONS ON POWER ELECTRONICS and the IEEE JOURNAL ON EMERGING AND SELECTED TOPICS ON POWER ELECTRONICS. He has been the Guest Editor of several IEEE journal special issues and has organized many IEEE conference special sessions. He currently serves as the Vice-Chair of the IEEE IAS Industrial Lighting and Displays Committee. He is a Member-at-Large of the IEEE IAS Executive Board, currently serving as the IAS Newsletter Editor, among other activities. He is a Member of the Power Electronics Technical Committee of the IEEE IES. He is also a Member of the European Power Electronics Association.